JACS
JOURNAL OF THE AMERICAN CHEMICAL SOCIETY
pubs.acs.org/JACS
Article

Precisely Programmable Degradation and Drug Release Profiles in Triblock Copolyether Hydrogels with Cleavable Acetal Pendants

Jinsu Baek, Nanhee Song, Byungwoo Yoo, Dongwon Lee, and Byeong-Su Kim*

Cite This: https://doi.org/10.1021/jacs.3c14838
Read Online

ABSTRACT: Hydrogels hold significant promise as drug delivery systems due to their distinct advantage of sustained localized drug release. However, the challenge of regulating the initial burst release while achieving precise control over degradation and drug-release kinetics persists. Herein, we present an ABA-type triblock copolymer-based hydrogel system with precisely programmable degradation and release kinetics. The resulting hydrogels were designed with a hydrophilic poly(ethylene oxide) midblock and a hydrophobic end-block composed of polyethers with varying ratios of ethoxyethyl glycidyl ether and tetrahydropyranyl glycidyl ether acetal pendant possessing different hydrolysis kinetics. This unique side-chain strategy enabled us to achieve a broad spectrum of precise degradation and drug-release profiles under mildly acidic conditions while maintaining the cross-linking density and viscoelastic modulus, which is unlike the conventional polyester-based backbone degradation system. Furthermore, programmable degradation of the hydrogels and release of active therapeutic agent paclitaxel loaded therein are demonstrated in an in vivo mouse model by suppressing tumor recurrence following surgical resection. Tuning of the fraction of two acetal pendants in the end-block provided delicate tailoring of hydrogel degradation and the drug release capability to achieve the desired therapeutic efficacy. This study not only affords a facile means to design hydrogels with precisely programmable degradation and release profiles but also highlights the critical importance of aligning the drug release profile with the target disease.

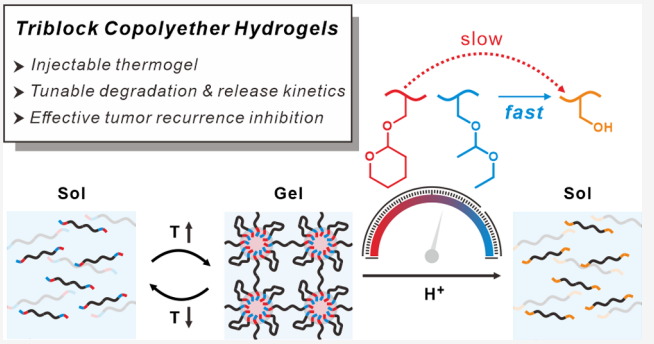

INTRODUCTION

Conventional therapeutics, including small molecule drugs, peptides, and proteins, often exhibit low solubility or a short circulatory lifetime.[1,2] These limitations necessitate frequent drug administration, which can cause patient discomfort, an increased risk of infection, and potential adverse side effects.[3,4] To address these challenges, an effective drug delivery system that significantly enhances solubility, prolongs drug circulation and consequently reduces the required drug dosage is imperative.[5−7] Among the various drug delivery systems currently available, hydrogels stand out as a unique and promising platform that offers advantages such as localized and sustained drug release.[8,9] Furthermore, their tissue-like mechanical properties and high water content enable hydrogels to be positioned near the target site without inducing severe foreign body reactions.[10−12] The elucidated advantages prove highly effective for postoperative care.[13] The hydrogel not only inherently prevents adhesion between tissues but also has been extensively investigated as a sustained drug delivery platform to mitigate the risk of infection or recurrence of diseases.[14,15]

However, precise programming of the drug release profile from hydrogels remains a formidable challenge. One issue arises from their porous structure coupled with a steep drug concentration gradient immediately after implantation, making it difficult to prevent an initial burst release of the loaded drug.[8,16,17] As a result, a significant proportion of the drug is initially released that can potentially exceed the toxic concentration threshold of the drug. Another issue relates to the varying duration of drug treatment depending on the symptoms of the disease and the type of drug; for instance, common bacterial infections often require 3 to 10 days of antimicrobial treatment whereas anticancer therapies can extend over months to years and chronic disease management may necessitate an even longer duration.[18−20] Consequently, there is an incessant demand to incorporate a wide range of drug release profiles into a drug delivery system to accommodate variation in the disease treatment duration. In this context, various approaches have been explored to address these issues, including the modification of cross-linking density to regulate simple diffusion,[21,22] drug conjugation within the

Received: December 31, 2023
Revised: April 25, 2024
Accepted: April 26, 2024

hydrogel network,[23−25] and incorporation of degradable cross-linkers.[26] However, modifying the cross-linking density can alter the mechanical properties of the hydrogel, thereby potentially causing a mechanical mismatch with the target tissue. In addition, while drug conjugation within the hydrogel network via degradable bonds can preserve the mechanical properties of hydrogels, it often requires additional functional groups and conjugation chemistry. Alternatively, incorporating degradable cross-linkers can provide an efficient way to alter the hydrogel degradation kinetics.

Nevertheless, effective prevention of the initial burst release resulting from exploiting a concentration gradient remains a significant challenge. To date, no straightforward solutions for preparing hydrogels with precisely programmable drug release profiles and preventing an initial burst release while maintaining their mechanical properties have been forthcoming. In our previous work, we introduced a new strategy to precisely control the hydrogel degradation kinetics using ABA-type triblock copolymers with hydrophobic acetal pendants (Scheme 1).[27] As the hydrolysis kinetics of the acetal groups is highly affected by the structure and the conformation of the monomer, hydrogels prepared from two different acetal-based monomers also display a distinct difference in degradation behavior.[28−30] It should be noted that after the hydrolysis of all pendant moieties, the A end-block turns into the linear polyglycerol which is well known for its high biocompatibility.[31] Given that low-molecular-weight PEO similar to that of our resulting triblock copolymer could be efficiently excreted from the body, the utilization of this system as a drug delivery carrier is compelling.[32] Furthermore, unlike the backbone cleavage system involved in polylactide (PLA), poly(lactide-*co*-glycolide) (PLGA), or poly(ε-caprolactone) (PCL), all of which have complicated degradation kinetics, cleavable pendants impart controllable and predictable dynamic properties.[33,34] While this prior work provided valuable insights into mechano-temporal transitions within the developed hydrogel system involving a single monomer, the relationship between hydrogel degradation and its release behavior of an active therapeutic agent remains unexplored.

Scheme 1. (Top) Schematic Illustration of a Thermo- and pH-Responsive ABA Triblock Copolymer Hydrogel and (bottom) a Comparison of the A End-Block Hydrolytic Degradation Mechanisms in the Polyester-Based Backbone Degradation and Mixed Acetal-Based Pendant Degradation Systems

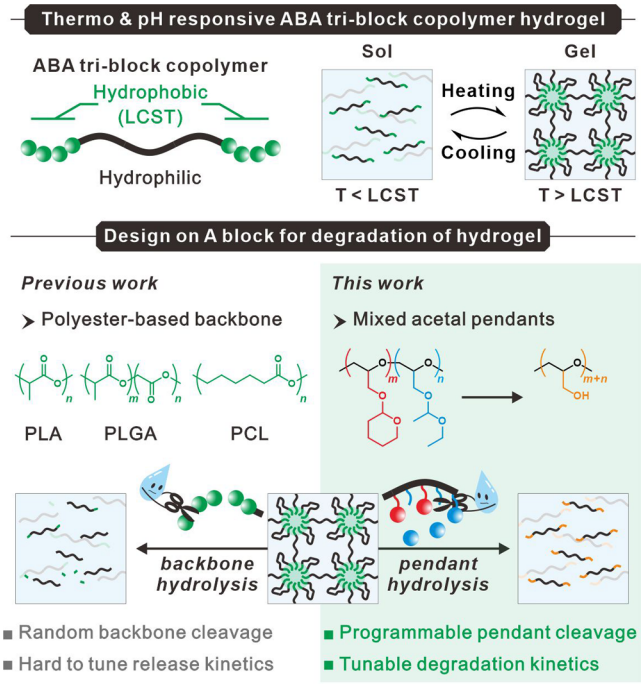

Inspired by this precedent work, we prepared poly(ethylene oxide) (PEO)-based triblock copolymers using varying fractions of two different acetal-based functional epoxide monomers. Specifically, ethoxyethyl glycidyl ether (EE) and tetrahydropyranyl glycidyl ether (TP) monomers were employed to prepare a series of all polyether-based triblock copolymers P(EE-*co*-TP)$_{x/y}$-*b*-PEO-*b*-P(EE-*co*-TP)$_{x/y}$ using PEO via anionic ring-opening polymerization (Scheme 2 and see Table 1 for details). The prepared triblock copolymers were carefully characterized using ^{1}H NMR, gel permeation chromatography (GPC), and differential scanning calorimetry (DSC). Moreover, a series of rheology and ex situ NMR studies were conducted to elucidate the mechanical properties and degradation and release kinetics of the prepared hydrogels. Furthermore, in vivo application of the hydrogels to a tumor-recurrence mouse model clearly demonstrated the precisely controllable degradation kinetics of the hydrogels to achieve a programmable drug release profile for the anticancer therapeutic agent to effectively eradicate any remaining tumors after surgery. Coupled with its superior biocompatibility, the precise programming of the degradation kinetics of the hydrogels further underscores the significance of fine-tuning the drug release profile of the hydrogels.

RESULTS AND DISCUSSION

Preparation of Triblock Copolymers. To examine the effect of tuning the relative fractions of EE and TP in the end-group in the triblock copolymers on the degradation and drug release profile of the resulting hydrogel, two functional epoxide monomers with acetal pendants were synthesized via simple hydroxyl protection chemistry and purified via fractional distillation according to previous reports (Figures 1a,b, and S1−S8).[35,36] A series of ABA-type triblock copolymers were prepared via anionic ring-opening polymerization using PEO (M_n = 20,000 g/mol) and *t*-Bu-P$_4$ as a macroinitiator and base, respectively. Here, metal-free organic phosphazene base *t*-Bu-P$_4$ was used, owing to its high basicity and, more importantly, its facile polymerization without side reactions. Various ratios of acetal functionalized epoxide monomers EE and TP were copolymerized to afford P(EE-*co*-TP)$_{x/y}$-*b*-PEO-*b*-P(EE-*co*-TP)$_{x/y}$ with various molar fractions of TP in the A end-block (f_{TP}), as provided in Table 1. The number in each sample, T$_n$, represents the percentage of TP in the A end-block. In addition, the degree of polymerization (DP) of each A end-block was set to 25 in this study to minimize the effects of molecular weight.

Characterization and purification were confirmed by a number of different techniques, including ^{1}H NMR, GPC, and DSC (Figures 1c and S9−S11). For example, the distinct methine peaks in the respective ^{1}H NMR spectra of EE and TP were used to calculate the EE/TP ratio after polymerization (Figure 1c). The relative fractions of EE and TP within the end block were readily controlled depending on the feed ratio of the monomers, given their reactivity ratios during the

https://doi.org/10.1021/jacs.3c14838
J. Am. Chem. Soc. XXXX, XXX, XXX−XXX

Scheme 2. (Top) Syntheses of Ethoxyethyl Glycidyl Ether (EE) and Tetrahydropyranyl Glycidyl Ether (TP) Monomers, Polymerization Using Poly(ethylene oxide) (PEO) as a Macroinitiator To Afford Triblock Copolymers P(EE-*co*-TP)$_{x/y}$-*b*-PEO-*b*-P(EE-*co*-TP)$_{x/y}$, and (Bottom) Demonstration of the Thermo- and pH-Responsive Properties, Injectability, and Programmable Degradation Kinetics of the Hydrogels

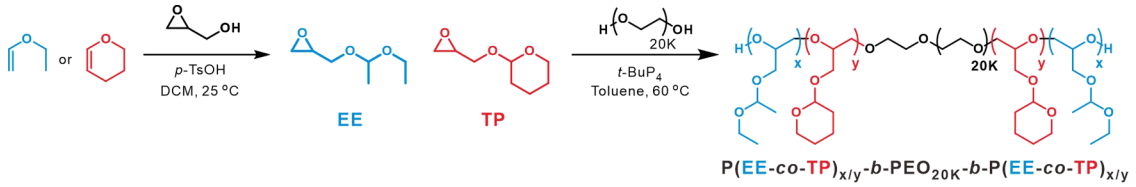

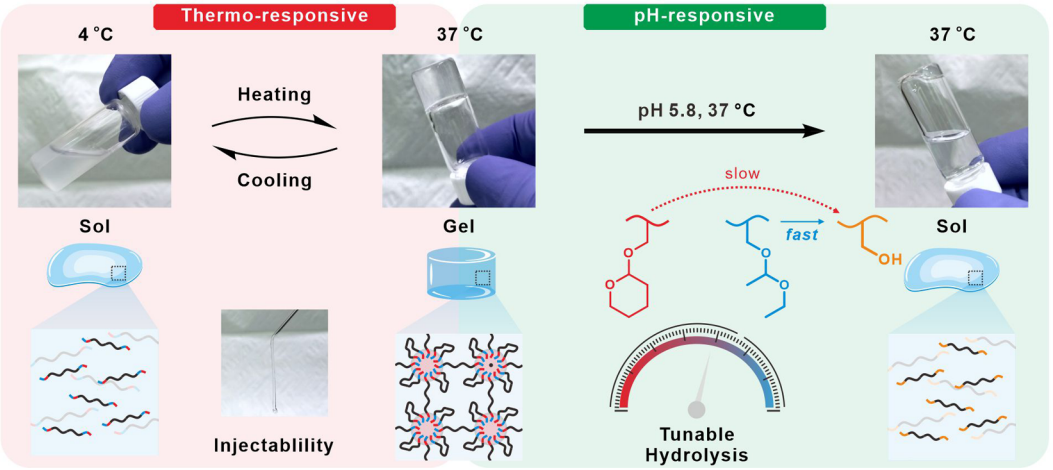

Table 1. Characterization Data of the Polymers and Hydrogels Prepared in This Study

entry	sample	DP_{NMR} [a]	f_{TP} [b]	$M_{n,NMR}$ [a] (g mol^{-1})	$M_{n,GPC}$ [c] (g mol^{-1})	$Đ$ [c]	T_g [d] (°C)	T_{gel} [e] (°C)
1	T_0	27	0.00	27,900	28,000	1.08	−62.0	32
2	T_{11}	26	0.11	27,500	26,300	1.12	−55.2	26
3	T_{27}	26	0.27	27,800	25,000	1.15	−49.4	21
4	T_{51}	25	0.51	27,600	26,300	1.11	−39.7	17
5	T_{79}	24	0.79	27,300	25,800	1.11	−29.4	4
6	T_{100}	27	1.00	28,500	25,000	1.12	−21.5	n.d.

[a]The degree of polymerization (DP) of each A end-block measured using ^{1}H NMR analysis. [b]The molar fraction of tetrahydropyranyl glycidyl ether (TP) in the A-block of each copolymer. [c]The molecular weight obtained via GPC calibrated using PEO/PEG standard in a DMF containing 0.10 wt % LiCl as the eluent, RI detector. [d]The molecular weight determined via using DSC at a scan rate of 10 °C min^{-1}. [e]Gelation temperature identified via temperature-sweep analysis. The polymer concentrations used were 7.5 wt % for T_0−T_{79} and 5 wt % for T_{100}, respectively.

copolymerization (r_{EE} = 1.49 ± 0.01 and r_{TP} = 0.69 ± 0.01, respectively), as determined via ex situ ^{1}H NMR analysis.[36] Furthermore, DSC measurements showed only a single glass transition temperature (T_g) for all of the polymers prepared irrespective of the EE/TP ratio, which verified the random copolymerization of A end-blocks that are fully miscible with the PEO midblock (Figure S9). This feature is beneficial in minimizing the phase separation behavior between the A and B blocks during hydrogel formation and degradation.

Meanwhile, side reactions such as self-initiation and cross-coupling between the polymers were not observed during polymerization, as indicated by the NMR and GPC spectra of the polymer set in Figures 1, S10, and S11. Notably, the molecular weights obtained from GPC ($M_{n,GPC}$) decreased as the hydrophobic characteristics of the end-block increased, while the molecular weights determined from NMR spectra ($M_{n,NMR}$) were in a similar range (Figure S11). This can be attributed to a decrease in the radius of gyration of the hydrophobic blocks in triblock copolyethers under GPC conditions, as has been similarly observed in previous studies.[35−37]

Preparation of Hydrogels and Their Temperature-Responsive Property. After characterization of the polymer set, the 7.5 wt % of triblock copolymers were incubated in phosphate-buffered saline (PBS) at pH 7.4 and 4 °C until fully dissolved; the incubation time was increased according to the hydrophobicity of the end-block. Specifically, T_0 became a homogeneous solution after 6 h, while it took more than 2 days for T_{79}. After the polymers were fully dissolved in the medium, the sol−gel transition behavior of the resulting hydrogels depending on the EE/TP ratio and temperature was investigated. As depicted in Scheme 2, the synthesized triblock copolymers underwent self-assembly in the aqueous medium to form hydrogels in which nanoscale A end-block cores were interconnected by PEO midblocks. Because the hydrophobic association is favored at elevated temperature due to the nature of the end-blocks possessing lower critical solution temperature (LCST) property, the formation of macroscopic three-dimensional networks through the A end-block core (i.e.,

https://doi.org/10.1021/jacs.3c14838
J. Am. Chem. Soc. XXXX, XXX, XXX−XXX

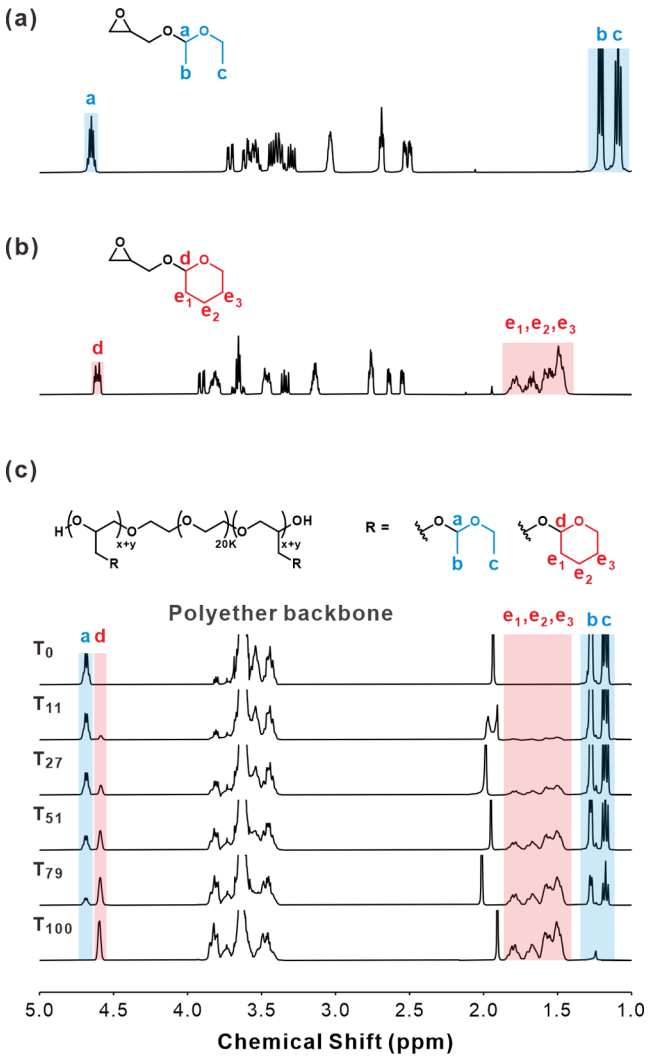

Figure 1. ^{1}H NMR spectra of (a) ethoxyethyl glycidyl ether (EE) monomer, (b) tetrahydropyranyl glycidyl ether (TP) monomer, and (c) a series of resulting triblock copolymers, P(EE-*co*-TP)$_{x/y}$-*b*-PEO-*b*-P(EE-*co*-TP)$_{x/y}$, with varying fractions of each monomer in the end-block (see Table 1 for details). All of the spectra were measured at 25 °C (400 MHz, $CDCl_3$). See full assignments in the Supporting Information.

gelation) occurred at an elevated temperature (Figure 2a).[38,39] The LCST behaviors of each polymer were further characterized via dynamic light scattering measurement upon increasing temperature, suggesting a gradual transition from single chains to micelles and aggregates (Figure S12). From the temperature sweep analysis, we found that the T_0−T_{79} hydrogels exhibited the sol−gel transition under 37 °C (Figures 2b and S13). Increasing f_{TP} lowered the sol−gel transition temperature (T_{gel}) by increasing the hydrophobicity of the A-block. It is noteworthy that all of the hydrogels could form a gel-like structure lower than body temperature (37 °C), which would enable them to maintain their structure while releasing active therapeutics in vivo.

Although all of the hydrogels displayed similar viscoelastic moduli (Figure 2c), their relaxation times were distinctly different and significantly influenced by the f_{TP} (Figures 2d,e, and S14). In other words, the integrity of the micellar core could be readily tailored by modulating the EE/TP ratio while keeping the number of micellar junctions similar. Since it has been revealed that the mechano-temporal properties of a hydrogel can be tuned by regulating the end-block hydrophobicity,[40] we noticed a gradual increase in the stress relaxation times of hydrogels T_0 to T_{79} with increasing f_{TP}. Interestingly, the stress relaxation time and f_{TP} showed an exponential relationship (Figure 2f), which can be explained by the stress relaxation behavior of the triblock copolymer hydrogel being governed by the end-block pullout time ($\tau_{pullout}$) according to the following relationship[41]:

$$\tau_{pullout} = \tau_{Rouse} \times e^{\alpha\chi N_{end}} \quad (1)$$

where τ_{Rouse} is the rouse relaxation time modeled as $b^2N_{end}{}^2\zeta/6\pi^2k_bT$, in which b, ζ, k_b, and T represent the statistical segment length, the friction factor of the monomer, the Boltzmann constant, and the temperature, and α, χ, and N_{end} mean an unknown factor, Florry−Huggins solubility parameter for each monomer and the DP of A-block, respectively. Specifically, $\alpha\chi N_{end}$ can be expressed as

$$\alpha\chi N_{end} = (\alpha\chi_{EE}N_{EE} + \alpha\chi_{TP}N_{TP}) \quad (2)$$

By assuming that $N_{EE} + N_{TP}$ is 25, eq 2 can be rearranged to provide

$$\alpha\chi N_{end} = 25\{\alpha\chi_{EE} + (\alpha\chi_{TP} - \alpha\chi_{EE})f_{TP}\} \quad (3)$$

In addition, according to the study of Smith and co-workers,[42] the effective friction coefficient of the A-block consisting of EE and TP can be written as

$$\zeta_{eff} = \zeta_{EE^\circ}{}^{f_{EE}}\zeta_{TP^\circ}{}^{f_{TP}} \quad (4)$$

where ζ_{EE° and ζ_{TP°, and f_{EE} and f_{TP} are the monomeric friction factors and volume fractions of EE and TP, respectively. Considering that the volumes of EE and TP are similar, eq 4 can be rewritten by replacing f_{EE} with $f_{EE} = 1 - f_{TP}$ as follows:

$$\zeta_{eff} = \zeta_{EE^\circ}(\zeta_{TP^\circ}/\zeta_{EE^\circ})^{f_{TP}} \quad (5)$$

Thus, $\tau_{pullout}$ can be expressed as

$$\ln \tau_{pullout} = A \times f_{TP} + B \quad (6)$$

,where $A = \ln(\zeta_{TP^\circ}/\zeta_{EE^\circ}) + (\alpha\chi_{TP} - \alpha\chi_{EE})$ and $B = 25\alpha\chi_{EE} + \ln(b^2N_{end}{}^2\zeta_{EE^\circ}/6\pi^2k_bT)$ respectively.

The relaxation times of all of the hydrogels upon shear stress are represented by a single master curve in Figure 2e. Meanwhile, eq 6 further verifies the similar hydrogel formation mechanisms. Thus, all of the hydrogels exhibited gradual viscoelastic gel-to-sol transitions upon hydrolysis in a similar manner. Although adjustable stress relaxation behavior was not emphasized in this study, it holds significant potential in 3D cell culture and tissue engineering. We plan to employ our hydrogel system to regulate the morphology and differentiation efficiency of cells by continuously adjusting stress relaxation while maintaining stiffness.

pH-Responsive Tunable Degradation Rates of the Hydrogels. To confirm the tunable degradation behavior of the hydrogels depending on f_{TP}, they were immersed in mildly acidic phosphate buffer (pH 5.8). As shown in Figure 3a, the degradation mechanism of the hydrogels involves the stepwise hydrolysis of the inner core-block of the A end-blocks of the triblock copolymer hydrogels, including (i) core-block swelling, (ii) acidic hydrolysis, (iii) hydrophobic-to-hydrophilic transition of the A end-block, and (iv) chain pullout to full dissolution in solution. In particular, due to the presence of

https://doi.org/10.1021/jacs.3c14838
J. Am. Chem. Soc. XXXX, XXX, XXX−XXX

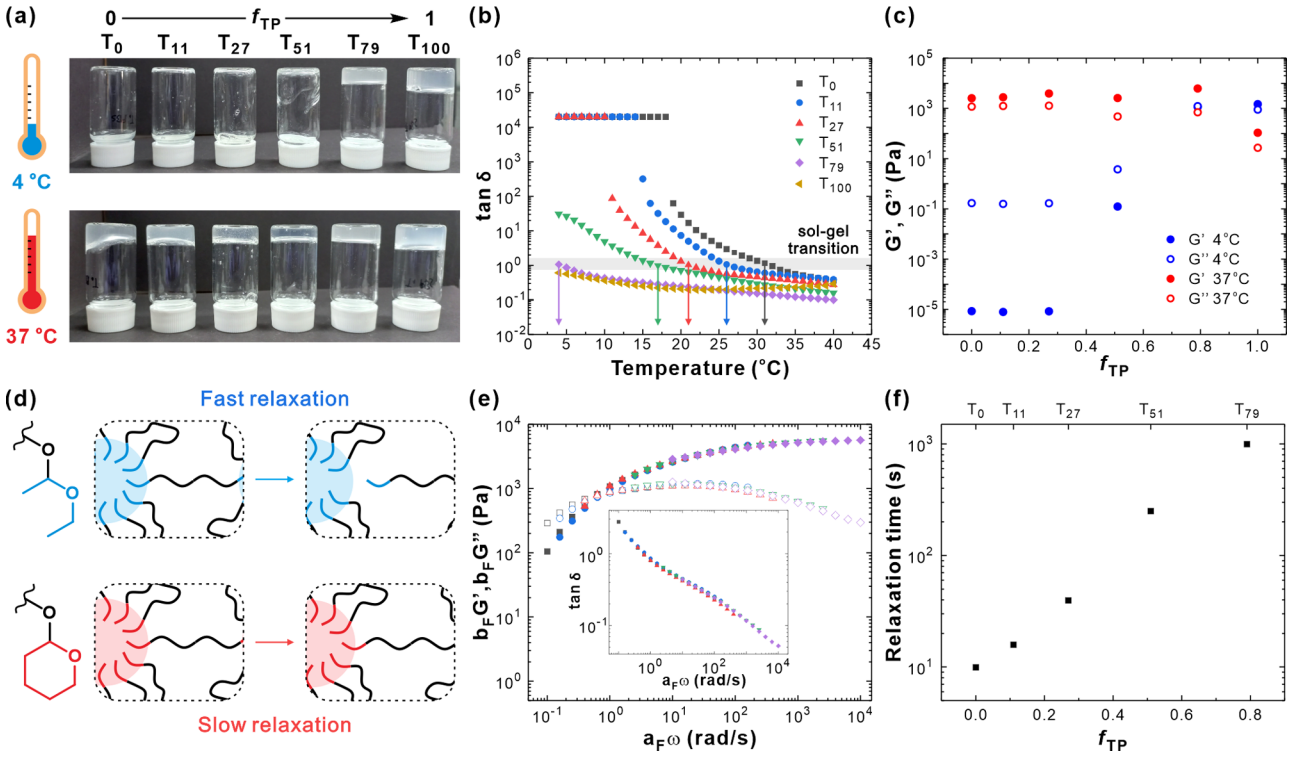

Figure 2. (a) Photographic images of the temperature responsive behavior of the hydrogels (7.5 wt % for T_0−T_{79} and 5.0 wt % for T_{100}) taken 30 s after vial inversion. (b) Temperature-sweep analysis and (c) comparison of the viscoelastic modulus of the hydrogels at 4 and 37 °C. The arrows represent the sol−gel transition temperature (10 rad/s, 1%). (d) A schematic illustration of the stress relaxation mechanism of hydrogels with different acetal pendant groups. (e) Time-f_{TP} superposition master curves of the dynamic moduli G' (solid) and G'' (open) with T_{27} as a reference. Horizontal and vertical shift factors, a_F and b_F were applied. The inset shows the loss factor (tan δ) values plotted as a function of the stress frequency, depending on the f_{TP} value of the A end-block. (f) Relaxation time of each hydrogel with varying f_{TP} in the A end-block. The frequency sweep analysis was conducted at 37 °C using 1% strain in the range of 0.1−100 rad.

two exocyclic cleavable C−O bonds in the acyclic acetal pendants in EE, rapid hydrolysis occurs first in these acyclic acetal pendants, followed by slower hydrolysis of the cyclic tetrahydropyranyl acetal pendants in TP.[27,28] From the images of the degraded hydrogels, it was obvious that the degradation kinetics of the hydrogels under mildly acidic conditions could be tuned by modulating the f_{TP} of the A-block (Figure 3b). While the structure of the hydrogels persisted in the initial stage, T_0 hydrogel degraded almost completely and exhibited a liquid-like behavior after 8 days of incubation whereas T_{11} hydrogel still retained its gel-like behavior. This observation indicates that even subtle modulation of the A-block (i.e., f_{TP} from 0 to 0.11) can effectively tailor the rate of hydrolysis and the rheological properties of the hydrogel. Ex situ NMR analysis was performed to further elucidate whether the degradation of the hydrogel aligns with the hydrolysis of the hydrophobic acetal pendant groups. The representative *ex situ* NMR spectra of T_{27} shown in Figure 3c demonstrate that the overall integration values of the acetal pendant groups with reference to the polyether backbone clearly decreased over time. Furthermore, the acyclic acetal pendants in the EE block exhibited a rapid reduction compared to the cyclic pendants in the TP block, which aligns with the proposed degradation mechanism. In addition, the visual degradation behavior according to f_{TP} was well synchronized with the percentage of hydrolyzed acetal pendants identified from the ex situ NMR study (Figure 3d). This result further highlights that the degradation kinetics of the hydrogel can be precisely tuned by simply adjusting f_{TP} in the A end-block.

Encouraged by the precisely programmable degradation of the hydrogels, we carried out model drug loading and release analyses to determine the drug release profile of the triblock copolymer hydrogel system. Given that triblock copolymer hydrogels possess a large hydrophobic core that is interconnected by hydrophilic PEO spacers, the hydrophobic pocket was exploited to load hydrophobic small molecules. Specifically, a solvent-casting method was employed to encapsulate the model drug Nile Red into the hydrogels.[43,44] Afterward, the hydrogels were immersed in phosphate buffer at pH 5.8 to induce their degradation and subsequent release of the model drug, which was measured by monitoring the photoluminescence of the supernatant for 15 days (Figure 4a). It was observed that there was an initial induction period that resisted wetting of the core block, thus retarding hydrolysis of the acetal-based pendant groups, followed by a relatively gradual increase in the release of the model drug in the order of T_0, T_{11}, and T_{27}, which is in accordance with their degradation rates. It is of note that neither the T_{51} nor T_{79} hydrogel released a noticeable amount of the model drug due to the considerably low degree of degradation during the time of the test. In addition, the release of the model drug into the buffer medium was readily visualized over time (Figure 4b). Considering the highly hydrophobic nature of the model drug, we postulate that the model drug is released as if it were encapsulated within the triblock copolymer micelles in aqueous buffer media. This hypothesis was further verified by observing that the maximum emission wavelength of Nile Red released from the hydrogel was significantly lower than

https://doi.org/10.1021/jacs.3c14838
J. Am. Chem. Soc. XXXX, XXX, XXX−XXX

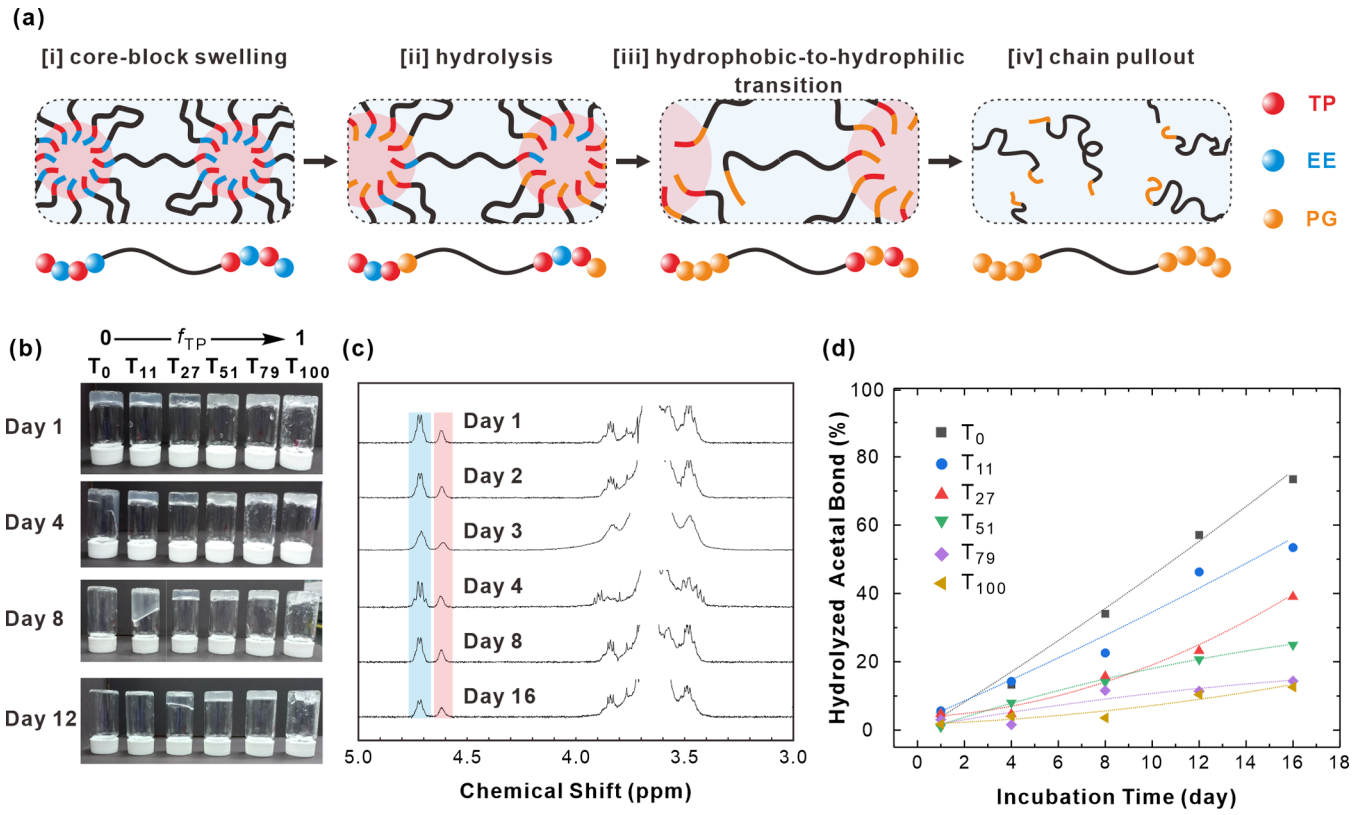

Figure 3. (a) Schematic illustration of the stepwise degradation mechanism of the prepared hydrogels upon hydrolysis. (b) Corresponding photographic images of the hydrogels degraded after various incubation periods in phosphate buffer (pH 5.8) taken 20 s after vial inversion. (c) Ex situ ^{1}H NMR spectra of the T_{27} hydrogel. (d) Comparison of the hydrolysis of the acetal pendants in all of the hydrogels upon incubation in pH 5.8 buffer for various periods. PG, polyglycidol; EE, ethoxyethyl glycidyl ether; and TP, tetrahydropyranyl glycidyl ether.

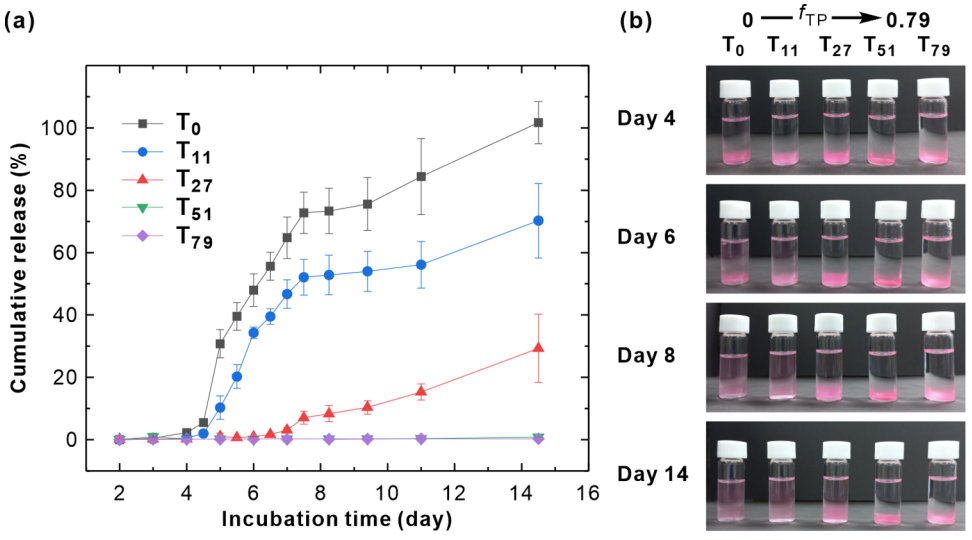

Figure 4. (a) Release profiles of the model drug Nile Red from the T_0−T_{79} hydrogels and (b) corresponding photographic images after incubation in mild acidic buffer (pH 5.8) for various periods. Note that the Nile Red release from the T_{51} and T_{79} hydrogels is not clearly discernible. The values are expressed as the mean and standard deviation (n = 3 for each set).

that in water (Figure S15). This might be the reason why initial burst release was not observed despite all hydrogels exhibiting a porous structure (Figure S16).

An additional release experiment with a real drug, paclitaxel (PTX) was performed to confirm that the hydrolysis of side pendants triggers the release of the drug inside (Figure S17). There was no release of PTX in neutral conditions, while a sustained release tendency was observed under mild acidic conditions. Therefore, it is evident that acid-catalyzed hydrolysis facilitates the release of PTX within the hydrogel. In hydrogels, there exists an equilibrium between the elastic force and swelling force by water inflow.[45] As the hydrolysis of the A-block resulted in a decrease in the relaxation time, the elastic force of the hydrogel became lower and broke the

https://doi.org/10.1021/jacs.3c14838
J. Am. Chem. Soc. XXXX, XXX, XXX−XXX

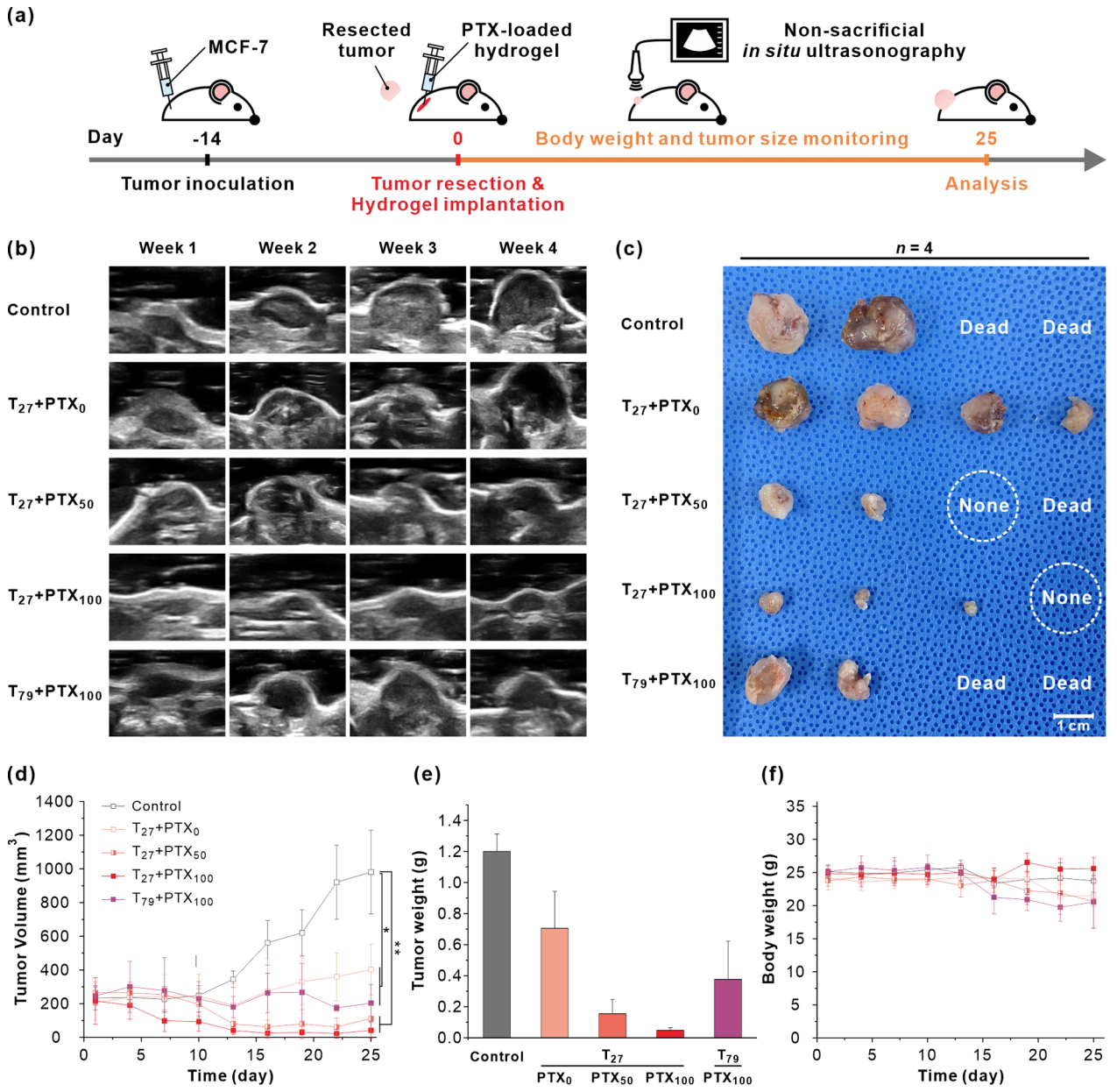

Figure 5. (a) Schematic illustration of the design of the in vivo tumor-recurrence mouse model. (b) Ultrasonography images to monitor tumor development and (c) a photographic image of the resected and collected tumors on day 25 (tumor disappearance and mouse mortality during the experiment are noted in the image). (d) Tumor volume changes after treatment with PTX-loaded T_{27} or T_{79} hydrogel (PTX_x designates the amount (μg) of PTX loaded into 100 μL of hydrogel (*$p < 0.05$, **$p < 0.01$ from two-sided Student's t-tests). (e) Final weight of the tumors and (f) body weight changes under various treatment conditions. Note that all values are expressed as the mean and standard deviation ($n = 4$ for each set).

equilibrium, ultimately resulting in the erosion of the polymers and micelles on the hydrogel surface. Taken together, the tunable degradation kinetics of the hydrogels clearly coincide with their small molecule release profiles, which highlights the significance of precisely programming the hydrogel-based system simply via fine-tuning of the monomer ratio in the end-block in this triblock copolymer system.

Anticancer Efficacy of the Hydrogel System in an In Vivo Postoperative-Tumor Recurrence Mouse Model. After the excellent biocompatibility of the hydrogel was confirmed through transwell analyses and MTT (Figures S18 and S19), a suitable disease model was selected to assess the critical role of degradation and release kinetics control. In this context, the hydrogel was employed to inhibit tumor recurrence following resection, which is frequently associated with residual tumor tissue.[46,47] The thermoresponsive property of the hydrogel can be exploited to conform to an irregular surface after surgery, while the mild acidic environment resulting from surgical inflammation facilitates the gradual degradation of the injected hydrogel.[48,49] By leveraging these attributes, we aimed to investigate the impact of the degradation and drug release kinetics of the hydrogel on therapeutic efficacy. Subsequently, we evaluated the therapeutic effects of PTX-loaded hydrogels on inhibiting postsurgical tumor recurrence using an MCF-7 xenograft mouse model. Following the surgical resection of tumors, the T_{27} and T_{79} hydrogels with varying amounts of PTX were implanted and postoperative-tumor recurrence and the anticancer efficacy of

https://doi.org/10.1021/jacs.3c14838
J. Am. Chem. Soc. XXXX, XXX, XXX−XXX

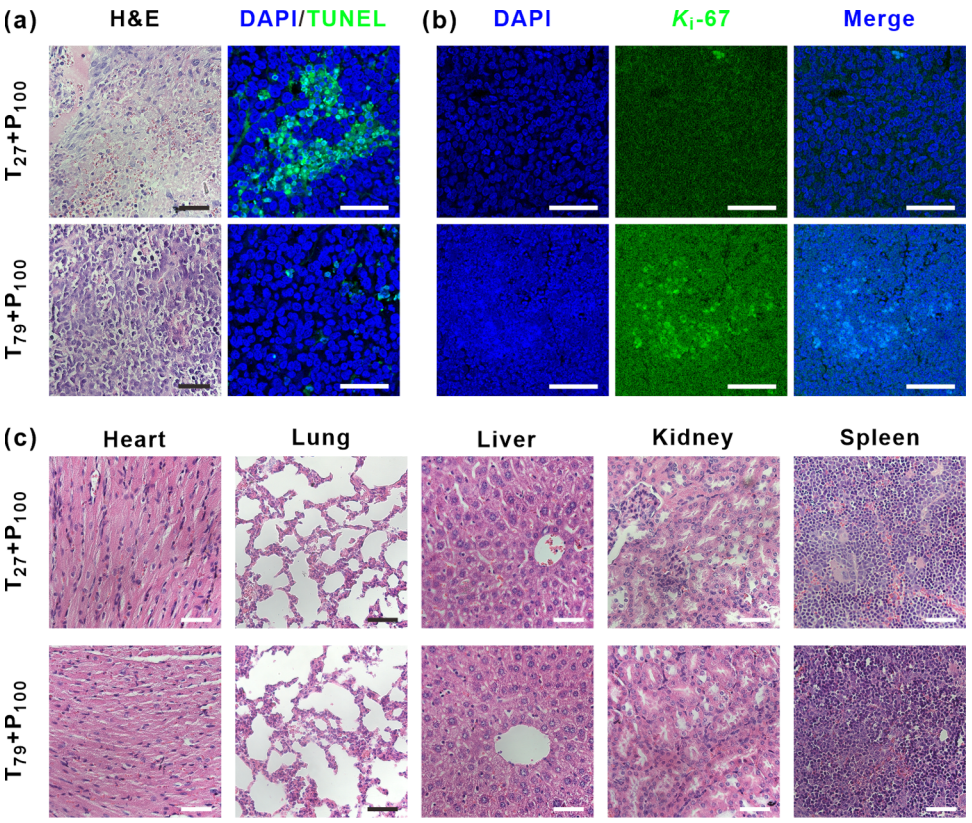

Figure 6. Histological examination of mouse tissues after treatment with PTX-loaded hydrogels for 25 days. Representative images of excised tumor tissue from mice treated with T_{27} + PTX_{100} or T_{79} + PTX_{100}: (a) (left) H&E and (right) DAPI and TUNEL staining (blue: DAPI; green: TUNEL) and (b) DAPI and K_i-67 immunofluorescence staining (blue: DAPI; green: K_i-67). (c) H&E-stained image sets of major organs from mice after treatment with T_{27} + PTX_{100} or T_{79} + PTX_{100} hydrogel for 25 days. All scale bars: 50 μm. H&E: hematoxylin and eosin; TUNEL: terminal deoxynucleotidyl transferase dUTP nick end-labeling.

the hydrogels were closely monitored by measuring the tumor volume and weight, and the body weight of the mice (Figure 5a). As shown in Figure 5b,d, the continuous progression of tumor recurrence was clearly visualized via noninvasive ultrasonography. After 25 days of monitoring, all of the mice were sacrificed, and tumors therein were resected again. Noticeably, the size and mass of the resected tumors were well aligned with the results obtained via ultrasonography, which demonstrates the effectiveness of the latter for in situ tumor-volume monitoring (Figure 5b,c,e). While rapid tumor growth was observed in the control group, marked tumor-recurrence inhibition was observed in the groups treated with the hydrogel samples. Interestingly, T_{27} + PTX_{100} (i.e., T_{27} hydrogel loaded with 100 μg of PTX) almost completely suppressed postsurgical tumor recurrence whereas the effect of T_{79} + PTX_{100} was marginal (Figure 5c,e). This can be explained by the difference in the degradation and release kinetics of the T_{27} and T_{79} hydrogels. As the degradation and the subsequent release of PTX from the T_{27} hydrogel began within 5 days, PTX inside the T_{27} hydrogel could be delivered to the remaining tumor tissue within a reasonable time scale. Meanwhile, since the release kinetics of the T_{79} hydrogel are much slower than those of the T_{27} hydrogel, the prolonged release time scale for the latter resulted in ineffective temporal delivery of PTX to the target tissue. Furthermore, the body weights of all of the mice were maintained, which highlighted the excellent biocompatibility of the hydrogel (Figure 5f).

Anticancer Efficacy of the PTX-Loaded Hydrogel. To further substantiate the postoperative anticancer effect of the PTX-loaded hydrogels, we collected sections of tumor tissues and stained them with hematoxylin and eosin (H&E) or K_i-67 (an immunofluorescence cell proliferation marker) (Figures 6a, b, S20 and S21). While large tumor cells with uniform nuclear distribution were observed in the control group, those from the groups treated with T_{27} + PTX_{50} or T_{27} + PTX_{100} showed disruption of their structures and nuclear shrinkage (Figure S20). Furthermore, the highest population of TUNEL-positive cells was observed in the group treated with T_{27} + PTX_{100}. This indicates that PTX released from the T_{27} hydrogel, as suggested by the results from the degradation and release assays, induced apoptotic cell death to suppress tumor recurrence. To further verify the efficacy of the PTX-loaded hydrogels on tumor cell recurrence, tumor tissues were stained with K_i-67 and K_i-67-positive cells indicated that PTX released from the hydrogel exerted highly potent anticancer activity that inhibited tumor recurrence.

Since biocompatibility is a crucial factor for the applicability of implantable materials, major organs were examined after treatment with T_{27} + PTX_{100} and T_{79} + PTX_{100}. Noticeably, no specific abnormalities were observed in tissues excised from the heart, lung, liver, spleen, or kidney (Figure 6c). Besides, the biochemistry assay revealed that neither the T_{27} nor T_{79} hydrogel induced a noticeable effect on hepatic functionality, as evidenced by moderate changes in the serum levels of aspartate aminotransferase (ALT) and alanine aminotransferase (AST) remaining within the accepted normal ranges (Figure S22). Thus, the excellent biocompatibility of the T_{27}

https://doi.org/10.1021/jacs.3c14838
J. Am. Chem. Soc. XXXX, XXX, XXX−XXX

and T_{79} hydrogels demonstrates their potential in clinical translation.

CONCLUSIONS

A thermo- and pH-responsive ABA-type triblock copolyether-based hydrogel with highly tunable degradation and release kinetics was demonstrated in this study. Anionic ring-opening polymerization enabled the precise copolymerization of EE and TP monomers comprising the A end-block by using PEO as a macroinitiator. The series of prepared hydrogels showed distinct differences in degradation and release kinetics with respect to f_{TP}, as confirmed via rheological and ex situ NMR studies, as well as a model dye release analysis. After confirming the biocompatibility of the polymer, the resulting hydrogels were loaded with PTX, and their postoperative-tumor recurrence inhibition efficiency was demonstrated. Notably, the PTX-loaded T_{27} hydrogel showed higher efficacy for the inhibition of tumor recurrence than did the T_{79} hydrogel with identical PTX loading. This result further highlights the importance of matching the degradation and release time scale of the drug delivery system to that of the target disease. Hence, we anticipate that this approach to finely tuning the degradation and release kinetics of hydrogels will play a pivotal role in advancing the development of sophisticated drug delivery systems, thereby offering significant promise for their applicability in the fields of biology and biomedicine.

ASSOCIATED CONTENT

Supporting Information

The Supporting Information is available free of charge at https://pubs.acs.org/doi/10.1021/jacs.3c14838.

Detailed experimental protocol; materials and instruments; NMR, GPC, DSC, DLS, additional rheometer analyses data, SEM image sets, raw emission spectra, release profiles of PTX, transwell analysis, MTT assay, TUNEL and K_i-67 staining images, and ALT and AST assays (PDF)

AUTHOR INFORMATION

Corresponding Author

Byeong-Su Kim − *Department of Chemistry, Yonsei University, Seoul 03722, Republic of Korea;* orcid.org/0000-0002-6419-3054; Email: bskim19@yonsei.ac.kr

Authors

Jinsu Baek − *Department of Chemistry, Yonsei University, Seoul 03722, Republic of Korea;* orcid.org/0000-0002-6393-9176

Nanhee Song − *Department of Polymer Nano Science and Technology, Jeonbuk National University, Jeonju 54896, Republic of Korea*

Byungwoo Yoo − *Department of Chemistry, Yonsei University, Seoul 03722, Republic of Korea;* orcid.org/0009-0009-8721-2682

Dongwon Lee − *Department of Polymer Nano Science and Technology, Jeonbuk National University, Jeonju 54896, Republic of Korea*

Complete contact information is available at: https://pubs.acs.org/10.1021/jacs.3c14838

Author Contributions

The manuscript was written through contributions of all authors. All authors have given approval to the final version of the manuscript.

Notes

The authors declare no competing financial interest.

ACKNOWLEDGMENTS

We appreciate Prof. Soo-Hyung Choi at Hongik University for supporting the rheometer and Prof. Seyoung Kim at Dankook University for insightful discussion. This work was supported by the National Research Foundation of Korea (NRF-2021R1A2C3004978 and NRF-2021M3H4A1A04092882).

REFERENCES

(1) Savjani, K. T.; Gajjar, A. K.; Savjani, J. K. Drug Solubility: Importance and Enhancement Techniques. *ISRN Pharm.* **2012**, *2012*, No. 195727.

(2) Werle, M.; Bernkop-Schnürch, A. Strategies to Improve Plasma Half Life Time of Peptide and Protein Drugs. *Amino Acids* **2006**, *30*, 351−367.

(3) Cohen, J. Il-12 Deaths: Explanation and a Puzzle. *Science* **1995**, *270*, 908−908.

(4) Singh, J. A.; Cameron, C.; Noorbaloochi, S.; Cullis, T.; Tucker, M.; Christensen, R.; Ghogomu, E. T.; Coyle, D.; Clifford, T.; Tugwell, P.; et al. Risk of Serious Infection in Biological Treatment of Patients with Rheumatoid Arthritis: A Systematic Review and Meta-Analysis. *Lancet* **2015**, *386*, 258−265.

(5) Tibbitt, M. W.; Dahlman, J. E.; Langer, R. Emerging Frontiers in Drug Delivery. *J. Am. Chem. Soc.* **2016**, *138*, 704−717.

(6) Park, K. Controlled Drug Delivery Systems: Past Forward and Future Back. *J. Controlled Release* **2014**, *190*, 3−8.

(7) Kamaly, N.; Yameen, B.; Wu, J.; Farokhzad, O. C. Degradable Controlled-Release Polymers and Polymeric Nanoparticles: Mechanisms of Controlling Drug Release. *Chem. Rev.* **2016**, *116*, 2602−2663.

(8) Li, J.; Mooney, D. J. Designing Hydrogels for Controlled Drug Delivery. *Nat. Rev. Mater.* **2016**, *1*, 16071.

(9) Zhong, R.; Talebian, S.; Mendes, B. B.; Wallace, G.; Langer, R.; Conde, J.; Shi, J. Hydrogels for RNA Delivery. *Nat. Mater.* **2023**, *22*, 818−831.

(10) Spencer, K. C.; Sy, J. C.; Ramadi, K. B.; Graybiel, A. M.; Langer, R.; Cima, M. J. Characterization of Mechanically Matched Hydrogel Coatings to Improve the Biocompatibility of Neural Implants. *Sci. Rep.* **2017**, *7*, 1952.

(11) Zhang, Y.; An, D.; Pardo, Y.; Chiu, A.; Song, W.; Liu, Q.; Zhou, F.; McDonough, S. P.; Ma, M. High-Water-Content and Resilient PEG-Containing Hydrogels with Low Fibrotic Response. *Acta Biomater.* **2017**, *53*, 100−108.

(12) Guimarães, C. F.; Gasperini, L.; Marques, A. P.; Reis, R. L. The Stiffness of Living Tissues and Its Implications for Tissue Engineering. *Nat. Rev. Mater.* **2020**, *5*, 351−370.

(13) Cai, J.; Guo, J.; Wang, S. Application of Polymer Hydrogels in the Prevention of Postoperative Adhesion: A Review. *Gels* **2023**, *9*, 98.

(14) Liu, B.; Kong, Y.; Alimi, O. A.; Kuss, M. A.; Tu, H.; Hu, W.; Rafay, A.; Vikas, K.; Shi, W.; Lerner, M.; et al. Multifunctional Microgel-Based Cream Hydrogels for Postoperative Abdominal Adhesion Prevention. *ACS Nano* **2023**, *17*, 3847−3864.

(15) Qian, Q.; Wang, D.; Shi, L.; Zhang, Z.; Qian, J.; Shen, J.; Yu, C.; Zhu, X. A Pure Molecular Drug Hydrogel for Post-Surgical Cancer Treatment. *Biomaterials* **2021**, *265*, No. 120403.

(16) Jeong, B.; Bae, Y. H.; Kim, S. W. Drug Release from Biodegradable Injectable Thermosensitive Hydrogel of PEG−PLGA−PEG Triblock Copolymers. *J. Controlled Release* **2000**, *63*, 155−163.

(17) Huang, X.; Brazel, C. S. On the Importance and Mechanisms of Burst Release in Matrix-Controlled Drug Delivery Systems. *J. Controlled Release* **2001**, *73*, 121−136.

(18) Goodman, R. A.; Posner, S. F.; Huang, E. S.; Parekh, A. K.; Koh, H. K. Defining and Measuring Chronic Conditions: Imperatives for Research, Policy, Program, and Practice. *Prev. Chronic Dis.* **2013**, *10*, E66.
(19) Haslam, A.; Olivier, T.; Thawani, R.; Prasad, V. Duration of Treatment in Oncology Clinical Trials: Does the Duration Change When the Same Drug Moves from the Experimental Arm to the Control Arm? *ESMO Open* **2022**, *7*, No. 100480.
(20) Wilson, H. L.; Daveson, K.; Del Mar, C. B. Optimal Antimicrobial Duration for Common Bacterial Infections. *Aust. Prescr.* **2019**, *42*, 5−9.
(21) Kilic Boz, R.; Aydin, D.; Kocak, S.; Golba, B.; Sanyal, R.; Sanyal, A. Redox-Responsive Hydrogels for Tunable and "On-Demand" Release of Biomacromolecules. *Bioconjugate Chem.* **2022**, *33*, 839−847.
(22) Lust, S. T.; Hoogland, D.; Norman, M. D. A.; Kerins, C.; Omar, J.; Jowett, G. M.; Yu, T. T. L.; Yan, Z.; Xu, J. Z.; Marciano, D.; et al. Selectively Cross-Linked Tetra-PEG Hydrogels Provide Control over Mechanical Strength with Minimal Impact on Diffusivity. *ACS Biomater. Sci. Eng.* **2021**, *7*, 4293−4304.
(23) Ashley, G. W.; Henise, J.; Reid, R.; Santi, D. V. Hydrogel Drug Delivery System with Predictable and Tunable Drug Release and Degradation Rates. *Proc. Natl. Acad. Sci. U. S. A.* **2013**, *110*, 2318−2323.
(24) Henise, J.; Hearn, B. R.; Ashley, G. W.; Santi, D. V. Biodegradable Tetra-PEG Hydrogels as Carriers for a Releasable Drug Delivery System. *Bioconjugate Chem.* **2015**, *26*, 270−278.
(25) Schneider, E. L.; Henise, J.; Reid, R.; Ashley, G. W.; Santi, D. V. Hydrogel Drug Delivery System Using Self-Cleaving Covalent Linkers for Once-a-Week Administration of Exenatide. *Bioconjugate Chem.* **2016**, *27*, 1210−1215.
(26) Wang, Y.; Zhang, S.; Benoit, D. S. W. Degradable Poly(ethylene glycol) (PEG)-Based Hydrogels for Spatiotemporal Control of Sirna/Nanoparticle Delivery. *J. Controlled Release* **2018**, *287*, 58−66.
(27) Baek, J.; Kim, S.; Son, I.; Choi, S.-H.; Kim, B.-S. Hydrolysis-Driven Viscoelastic Transition in Triblock Copolyether Hydrogels with Acetal Pendants. *ACS Macro Lett.* **2021**, *10*, 1080−1087.
(28) Deslongchamps, P.; Dory, Y. L.; Li, S. The Relative Rate of Hydrolysis of a Series of Acyclic and Six-Membered Cyclic Acetals, Ketals, Orthoesters, and Orthocarbonates. *Tetrahedron* **2000**, *56*, 3533−3537.
(29) Liu, B.; Thayumanavan, S. Substituent Effects on the pH Sensitivity of Acetals and Ketals and Their Correlation with Encapsulation Stability in Polymeric Nanogels. *J. Am. Chem. Soc.* **2017**, *139*, 2306−2317.
(30) Shenoi, R. A.; Narayanannair, J. K.; Hamilton, J. L.; Lai, B. F. L.; Horte, S.; Kainthan, R. K.; Varghese, J. P.; Rajeev, K. G.; Manoharan, M.; Kizhakkedathu, J. N. Branched Multifunctional Polyether Polyketals: Variation of Ketal Group Structure Enables Unprecedented Control over Polymer Degradation in Solution and within Cells. *J. Am. Chem. Soc.* **2012**, *134*, 14945−14957.
(31) Thomas, A.; Müller, S. S.; Frey, H. Beyond Poly(ethylene glycol): Linear Polyglycerol as a Multifunctional Polyether for Biomedical and Pharmaceutical Applications. *Biomacromolecules* **2014**, *15*, 1935−1954.
(32) Yamaoka, T.; Tabata, Y.; Ikada, Y. Distribution and Tissue Uptake of Poly(ethylene glycol) with Different Molecular Weights after Intravenous Administration to Mice. *J. Pharm. Sci.* **1994**, *83*, 601−606.
(33) Li, J.; Stayshich, R. M.; Meyer, T. Y. Exploiting Sequence to Control the Hydrolysis Behavior of Biodegradable PLGA Copolymers. *J. Am. Chem. Soc.* **2011**, *133*, 6910−6913.
(34) Petit, A.; Müller, B.; Bruin, P.; Meyboom, R.; Piest, M.; Kroon-Batenburg, L. M. J.; de Leede, L. G. J.; Hennink, W. E.; Vermonden, T. Modulating Rheological and Degradation Properties of Temperature-Responsive Gelling Systems Composed of Blends of PCLA−PEG−PCLA Triblock Copolymers and Their Fully Hexanoyl-Capped Derivatives. *Acta Biomater.* **2012**, *8*, 4260−4267.
(35) Song, J.; Palanikumar, L.; Choi, Y.; Kim, I.; Heo, T.-Y.; Ahn, E.; Choi, S.-H.; Lee, E.; Shibasaki, Y.; Ryu, J.-H.; et al. The Power of the Ring: A pH-Responsive Hydrophobic Epoxide Monomer for Superior Micelle Stability. *Polym. Chem.* **2017**, *8*, 7119−7132.
(36) Song, J.; Hwang, E.; Lee, Y.; Palanikumar, L.; Choi, S.-H.; Ryu, J.-H.; Kim, B.-S. Tailorable Degradation of pH-Responsive All Polyether Micelles Via Copolymerisation with Varying Acetal Groups. *Polym. Chem.* **2019**, *10*, 582−592.
(37) Son, I.; Lee, Y.; Baek, J.; Park, M.; Han, D.; Min, S. K.; Lee, D.; Kim, B.-S. pH-Responsive Amphiphilic Polyether Micelles with Superior Stability for Smart Drug Delivery. *Biomacromolecules* **2021**, *22*, 2043−2056.
(38) Ci, T.; Chen, L.; Yu, L.; Ding, J. Tumor Regression Achieved by Encapsulating a Moderately Soluble Drug into a Polymeric Thermogel. *Sci. Rep.* **2014**, *4*, 5473.
(39) Isono, T.; Miyachi, K.; Satoh, Y.; Sato, S.-I.; Kakuchi, T.; Satoh, T. Design and Synthesis of Thermoresponsive Aliphatic Polyethers with a Tunable Phase Transition Temperature. *Polym. Chem.* **2017**, *8*, 5698−5707.
(40) Jung, H.; Gang, S.-E.; Kim, J.-M.; Heo, T.-Y.; Lee, S.; Shin, E.; Kim, B.-S.; Choi, S.-H. Regulating Dynamics of Polyether-Based Triblock Copolymer Hydrogels by End-Block Hydrophobicity. *Macromolecules* **2020**, *53*, 10339−10348.
(41) Peters, A. J.; Lodge, T. P. Comparison of Gel Relaxation Times and End-Block Pullout Times in A Triblock Copolymer Networks. *Macromolecules* **2016**, *49*, 7340−7349.
(42) Chapman, B. R.; Hamersky, M. W.; Milhaupt, J. M.; Kostelecky, C.; Lodge, T. P.; von Meerwall, E. D.; Smith, S. D. Structure and Dynamics of Disordered Tetrablock Copolymers: Composition and Temperature Dependence of Local Friction. *Macromolecules* **1998**, *31*, 4562−4573.
(43) Rao, D. A.; Nguyen, D. X.; Mishra, G. P.; Doddapaneni, B. S.; Alani, A. W. G. Preparation and Characterization of Individual and Multi-Drug Loaded Physically Entrapped Polymeric Micelles. *J. Vis. Exp.* **2015**, No. 102, No. e53047.
(44) Stammet, M.; Kwon, G. S.; Rao, D. A. Drug Loading in Pluronic® Micelles Made by Solvent Casting and Equilibrium Methods Using Resveratrol as a Model Drug. *J. Controlled Release* **2010**, *148*, e50−e51.
(45) Na, H.; Kang, Y.-W.; Park, C. S.; Jung, S.; Kim, H.-Y.; Sun, J.-Y. Hydrogel-Based Strong and Fast Actuators by Electroosmotic Turgor Pressure. *Science* **2022**, *376*, 301−307.
(46) Demicheli, R.; Retsky, M. W.; Hrushesky, W. J. M.; Baum, M.; Gukas, I. D. The Effects of Surgery on Tumor Growth: A Century of Investigations. *Ann. Oncol.* **2008**, *19*, 1821−1828.
(47) Lukianova-Hleb, E. Y.; Kim, Y.-S.; Belatsarkouski, I.; Gillenwater, A. M.; O'Neill, B. E.; Lapotko, D. O. Intraoperative Diagnostics and Elimination of Residual Microtumours with Plasmonic Nanobubbles. *Nat. Nanotechnol.* **2016**, *11*, 525−532.
(48) Jason, H.; Ken, B. J. Mechanism of Action of HTX-011: A Novel, Extended-Release, Dual-Acting Local Anesthetic Formulation for Postoperative Pain. *Reg. Anesth. Pain Med.* **2020**, *45*, 1030−1031.
(49) Zhuang, B.; Chen, T.; Xiao, Z.; Jin, Y. Drug-Loaded Implantable Surgical Cavity-Adaptive Hydrogels for Prevention of Local Tumor Recurrence. *Int. J. Pharm.* **2020**, *577*, No. 119048.

https://doi.org/10.1021/jacs.3c14838
J. Am. Chem. Soc. XXXX, XXX, XXX−XXX